REAR-SIDE POINT-CONTACTS BY INLINE THERMAL EVAPORATION OF ALUMINUM

Christoph Mader [1], Jens Müller [1], Sebastian Gatz [1], Thorsten Dullweber [1], and Rolf Brendel [1, 2]
[1] Institute for Solar Energy Research Hamelin (ISFH), Am Ohrberg 1, 31860 Emmerthal, Germany
[2] Institute for Solid-State Physics, Universität Hannover, Appelstrasse 2, 30167 Hannover, Germany

ABSTRACT

This paper presents a detailed analysis of point-contacted aluminum rear-sides for silicon solar cells that are metalized by inline thermal evaporation. We deposit aluminum layers of 2 µm thickness at dynamic deposition rates of 1.0, 2.9 and 5.0 µm*m/min on partially laser ablated a-Si / SiN passivation layers. The specific contact resistance of aluminum to *p*-type silicon with a doping density of 1×10^{16} cm^{-3} is determined to be 7.4 ± 1.2 $m\Omega cm^2$. Using the dynamic infrared lifetime mapping technique we measure effective lifetimes on the metalized samples of 300 cm/s at a metallization fraction of 3%. Simulations show a relative improvement of energy conversion efficiency of 0.6% over silicon solar cells featuring a screen printed aluminum rear-side metallization.

INTRODUCTION

Evaporation of metal for the formation of contacts to silicon solar cells is so far known as a high-efficiency laboratory technique.[1] Nevertheless high throughput inline evaporation systems have recently been investigated.[2] The rear-side of solar cells that are metalized by evaporation require a surface passivation layer and local contacts that cover only a small area to achieve high energy conversion efficiencies. A point-contact geometry results (Fig. 1). In this paper effective surface recombination velocities are measured on locally laser-opened, metalized double layer of a-Si / SiN. The specific contact resistance of deposited aluminum to *p*-type silicon is presented. We use experimental surface recombination velocities and contact resistance in one-dimensional solar cell device simulations to find the optimum contact geometry.

EXPERIMENTAL

We use 125 x 125 mm^2 single-crystalline 100-oriented 200 µm thick, B-doped, float-zone silicon wafers of 1.5 Ωcm resistivity and fabricate 9 structures of 30 x 30 mm^2 on each wafer as listed in Table I. The wafers are processed as follows. After KOH etching and RCA cleaning we deposit a 50 nm thick a-Si layer by means of remote-plasma enhanced chemical vapor deposition (PECVD) in a Plasmalab 80 PECVD reactor from Oxford Plasma Technology followed by a 100 nm thick PECVD SiN_x layer of a refraction index of 2.05 on both sides of the silicon wafer. The deposition parameters are described elsewhere.[3] According to the values in Table I, the passivated structure 2 through structure 9 are locally opened with a Nd: YVO4 laser of a pulse-duration of 8 to 9 picoseconds.

Table I: Description of the 9 structures on the 125 x 125 mm^2 wafer. Passivated refers to the surface passivation applying a stack of a-Si / SiN, *f* describes the metallization fraction of the surface, where the passivation layer was removed and the Al-layer is in direct contact with the Si-surface. The period length *p* refers to the distance between the point-contacts.

Structure	Description	Structure	Description
1	Non passivated	2	Passivated Not opened
3	Passivated *f*=42 % *p*=60 µm	4	Passivated *f*=4 % *p*=195 µm
5	Passivated *f*=2 % *p*=275 µm	6	Passivated *f*=0.25 % *p*= 780 µm
7	Passivated *f*=0.15 % *p*=1000 µm	8	Passivated *f*=0.07 % *p*=1500 µm
9	Passivated *f*=0.02 % *p*=2500 µm		

The metallization fraction $f = (\pi \times r^2) / p^2$ is determined via contact radius *r* and period length *p* (see Fig. 1) and varies from 0.02 % to 42 % by varying the period length from 2500 µm to 60 µm. The radius of the point-contacts is of 22 ± 2 µm. Contact radius *r* and period length *p* are determined via light microscope.

Table II: Deposition parameters for the single Al-deposition at the ATON 500 system.

Process	Dynamic deposition rate [µm*m/min]	Al layer thickness [µm]
1	1	2
2	2.9	2
3	5	2

Using the ATON 500 inline metallization system, we deposit aluminum layers of 2 µm thickness at dynamic deposition rates of 1.0, 2.9 and 5.0 µm*m/min. The deposition parameters are shown in Table II.
Subsequently we deposit a low temperature 200 nm thick PECVD SiN_x layer of a refractive index of 1.9 on the aluminum layer and ablate a complementary finger

structure of the SiN_x, again using our ps-laser system. Then we obtain with a following etching bath (boiling 37 % hydrochloric acid) a finger-structure that is used for the measurement of the specific contact resistance by the transfer length method (TLM).[4]

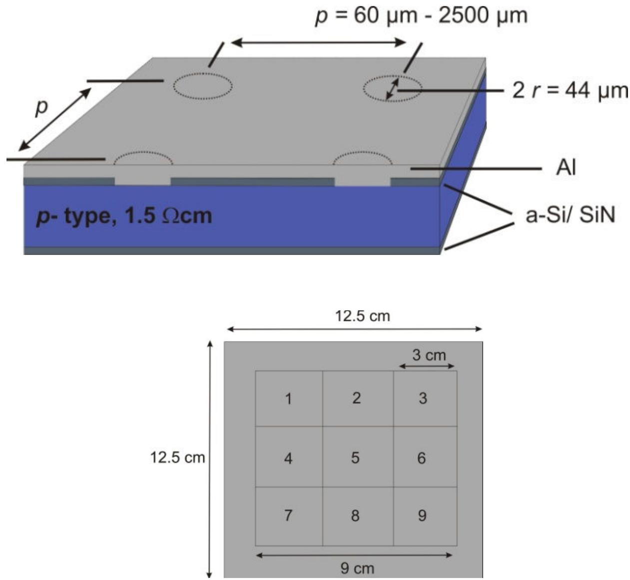

Figure 1: Schematic structure of silicon wafer with structures 1 through 9. The upper figure shows a cross-section of the local aluminum point-contacts with the diameter *r* and the period length *p*. The second figure shows the arrangement of the structures on the 125 x 125 mm² wafer. The structures are described in Table I.

For all lifetime measurements we use the dynamic infrared lifetime mapping (dynILM) technique[5,6]. All measurements are done at 0.3 suns. The dynILM allows us to measure the lifetime directly on metalized samples.

MEASURED CONTACT RESISTANCE AND SURFACE RECOMBINATION VELOCITY

Figure 2 shows the measured specific contact resistances ρ_c for the 3 dynamic deposition processes from Table II. A dynamic deposition rate of 5.0 µm*m/min shows the smallest contact resistance of 7.4 ± 1.2 mΩcm², whereas the processes of 1.0 µm*m/min and of 2.9 µm*m/min results in a contact resistance of 10.4 ± 1.2 mΩcm² and 11.8 ± 1.3 mΩcm², respectively. Note that the aluminum layers were not annealed after deposition, except for the thermal budget due to the deposition of the low-temperature SiN capping layer.

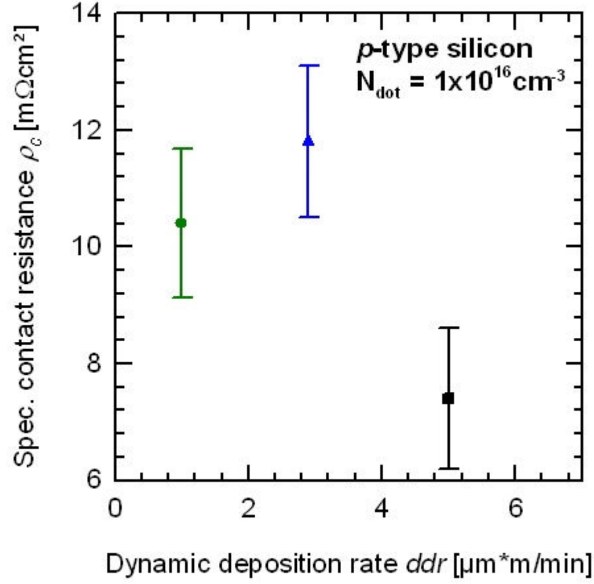

Figure 2: Specific contact resistance of inline-deposition processes 1 through 3, measured on the not passivated structure 1. Values are obtained using the transfer length method.

Surface recombination velocities are obtained from lifetime mapping measurements on partially metalized samples. Thus no further metal etching step after Al-deposition is necessary. From the measured injection dependent lifetime τ_{eff} we extract the effective SRV from the metalized side using the equation.[7]

$$\frac{1}{\tau_{\text{eff}}} = \frac{1}{\tau_{\text{bulk}}} + \frac{S_{\text{front}}}{W} + \frac{S_{\text{rear}}}{W} \quad (1)$$

For the bulk-lifetime τ_{bulk} we use the parameterization proposed by Kerr et al.[8] that accounts for Auger-recombination. For a 1.5 Ωcm boron-doped silicon wafer we calculate τ_{bulk} = 3.4 ms. The SRV on the front side S_{front} as obtained by dynILM on symmetric samples with Structure 2 results in S_{pass} = 2.2 ± 0.7 cm/s at an injection level of Δn = 7.5x10^{15} 1/cm³ for the a-Si:H passivated surfaces. On the completely metalized Structure 1 we deduce the recombination velocity under the contacts as S_{met} = 2.2x10^4 cm/s at Δn = 1.5x10^{12} 1/cm^3.

Figure 3 shows the measured SRV S_{eff} (symbols) of the 3 dynamic deposition rates depending on the period length.

The surface recombination velocity S_{eff} strongly reduces with increasing period length from 450 ± 16 cm/s for a period length of 195 µm to 3.8 ± 0.4 cm/s for a period length of 2500 µm due to the increased area fraction with high quality surface passivation. No significant difference in SRV is observed between the 3 deposition processes with rates of 1.0, 2.9 and 5.0 µm*m/min.

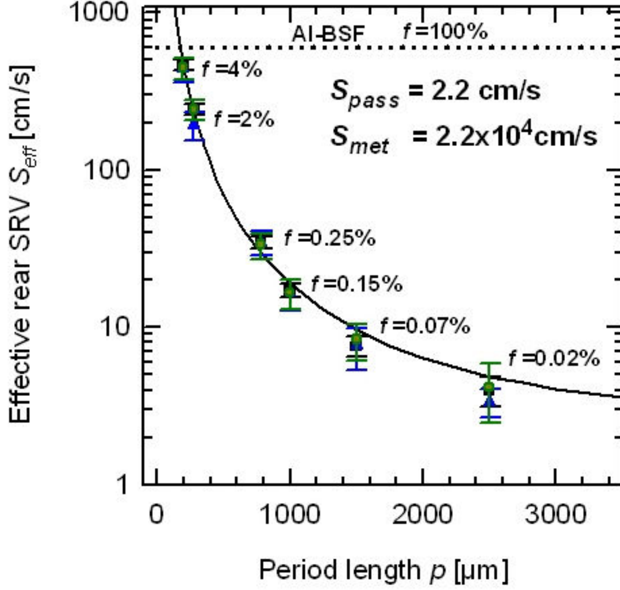

Figure 3: Effective surface recombination velocity of point-contacted surfaces of various period lengths and metallization fractions. Experimental data of the 3 deposition processes are represented by symbols. The solid line shows theoretical data calculated with equations (2) through (4).

MODELING

As the baseline case we consider a solar cell featuring a screen printed metallization processed at the ISFH. This solar cell is simulated using the one-dimensional simulation software PC-1D[9] with parameters shown in Table III.

Table III: Parameters used in the one-dimensional PC1D simulation

Parameter	Screen printed rear-side	Point-contacted rear-side
Front SRV [cm/s]	3×10^5	3×10^5
Emitter peak doping [cm^{-3}]	3.69×10^{20}	3.69×10^{20}
Emitter junction depth [nm]	105	105
Rear-reflectance [%]	70	90
Rear-SRV [cm/s]	1×10^6	Varying
BSF peak doping [cm^{-3}]	3×10^{18}	-
BSF junction depth [µm]	8	-

The measured and simulated energy conversion efficiency η of the cell featuring a screen printed metallization is 17.4%. We want to estimate the improvement of efficiency η by replacing the screen printed fully contacted rear-side by a passivated and locally contacted rear-side. The SRV and series-resistance of the carriers in the bulk of point-contacted solar cells is analytically described by a theory introduced by Fischer[10] that was extended by Plagwitz.[11] With S_{pass} being the SRV in the passivated area between the contacts and S_{met} being the SRV at the point-contacts the effective SRV results in

$$S_{\mathrm{eff}} = \frac{D}{\left\{\left(\frac{R_S}{\rho}+\frac{D}{fS_{\mathrm{met}}}\right)^{-1}+\left(\frac{\tilde{R}_S}{\rho}+\frac{D}{(1-f)S_{\mathrm{pass}}}\right)^{-1}\right\}^{-1}-W}. \qquad (2)$$

$$R_{\mathrm{s}} = p^2\frac{\rho}{2\pi r}\arctan\left(\frac{2W}{r}\right)+\rho W\left(1-\mathrm{e}^{-\frac{W}{p}}\right) \qquad (3)$$

is the series-resistance of the majority carriers in the bulk and depends on wafer-thickness W, specific-resistivity of silicon ρ, period length p and contact radius r.[10, 12]
$\tilde{R}_{\mathrm{s}}$ is the series resistance of the complementary structure of Fig. 1.

$$\frac{1}{\tilde{R}_{\mathrm{s}}} = \frac{1}{\rho W}-\frac{2\pi r}{\rho p^2\arctan\left(\frac{2W}{r}\right)\exp\left(\frac{W}{p}\right)} \qquad (4)$$

The solid line in Figure 3 displays the theoretical S_{eff} calculated from equation (2) through (4) and fits well to the measured values in the whole parameter range of the period length p.
We use Plagwitz' theory for modeling the efficiency of point-contacted solar cells. Simulated solar cell efficiencies η as a function of metallization fraction f for 3 contact radii of 22 µm, 100 µm and 500 µm are shown in Figure 4.

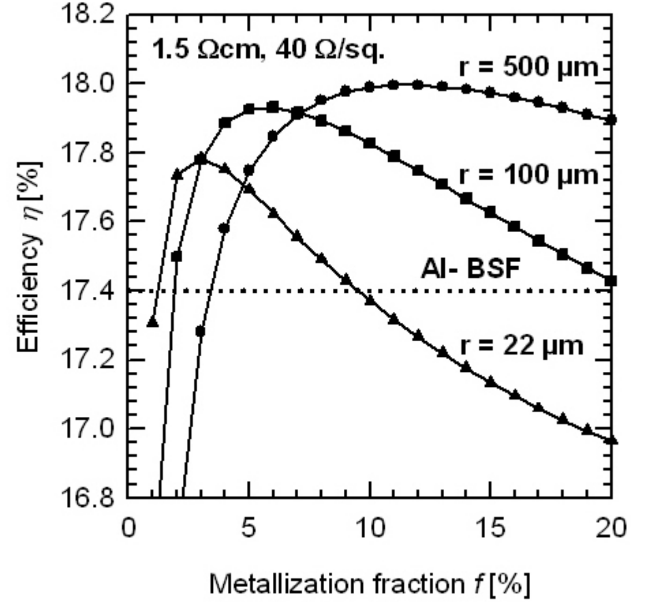

Figure 4: Energy conversion efficiency of point-contacted solar cells obtained by one-dimensional simulation. The simulation-parameters S_{eff} and R_s are calculated using equations (2) through (4) with S_{pass} = 2.2 cm/s and S_{met} = 2×10^4 cm/s. For comparison, the simulated energy conversion efficiency of a solar cell featuring a screen printed Al rear-contact is shown.

For comparison, the simulated energy conversion efficiency of the solar cell featuring a screen printed Al rear-contact is shown. The maximum efficiency as well as the optimum metallization-fraction f_{opt} of the point-contact solar cells increases with increasing opening radius *r* resp. metallization-fraction *f*. The simulated cell-efficiency η is limited by high series resistance for $f < f_{opt}$ and by increasing recombination at the rear surface for $f > f_{opt}$.
However, due to the better rear-reflectance and the lower surface recombination velocities, maximum efficiencies show an improvement of 0.6 % for the optimum contact geometry in comparison to a silicon solar cells featuring a screen printed rear-side metallization.

SUMMARY

In conclusion we show the high quality of solar cell contacts prepared by high throughput inline physical vapor deposition.
Specific contact resistance of Aluminum layers to Silicon of 7.4 mΩcm^2 directly after deposition is achieved. Surface recombination velocities of 300 cm/s on 3 % locally opened a-Si / SiN passivation stacks are measured. One-dimensional solar cell device simulations show an improvement of 0.6 % to a solar cell featuring a screen printed metallization.

ACKNOWLEDGEMENT

Funding was provided by the State of Lower Saxony and the German Ministry for the Environment, Nature Conservation, and Nuclear Safety (BMU) under Contract No. 0327666.

REFERENCES

[1] P. Engelhart, N.-P. Harder, T. Neubert, H. Plagwitz, B. Fischer, R. Meyer, R. Brendel, “Laser processing of 22% efficient back-contacted silicon solar cells”, 21st European Photovoltaic Solar Energy Conference, 2006, pp. 773- 776

[2] J. Nekarda, D. Reinwand, A. Grohe, P. Hartmann, R. Preu, R. Trassl, S. Wieder, “Industrial PVD Metallization for high efficiency crystalline silicon solar cells”, 34th IEEE Photovoltaic Specialists Conference, 2009, pp. 892-896

[3] S. Gatz, H. Plagwitz, P. Altermatt, B. Terheiden, R. Brendel, “Thermal stability of amorphous silicon/silicon nitride stacks for passivating crystalline silicon solar cells”, Applied Physics Letters, 2008, **93**, 173502

[4] H. H. Berger, “Models for contacts to planar devices”, Solid-State Electronics, 1972, **15**, pp. 145-158

[5] K. Ramspeck, S. Reissenweber, J. Schmidt, K. Bothe, R. Brendel, “Dynamic carrier lifetime imaging of silicon wafers using an infrared-camera-based approach”, Applied Physics Letters, 2008, **93**, 102104

[6] J. Müller, K. Bothe, S. Gatz, F. Haase, C. Mader, R. Brendel, (in preparation)

[7] D. E. Kane, and R. Swanson, “Measurement of the Emitter Saturation Current by a Contactless Photoconductivity Decay Method“, 18th IEEE Photovoltaic Specialist Conference, 1985, p 578

[8] M. Kerr, and A. Cuevas, “General parameterization of Auger recombination in crystalline silicon”, J. Appl. Phys., 2002, **91**, 2473

[9] P. Basore, D. Rover, and A. Smith, “PC-1D: Enhanced numerical solar cell modeling”, 20th IEEE Photovoltaic Specialist Conference, 1988

[10] B. Fischer, “Loss analysis of crystalline silicon cells using photoconductance and quantum efficiency measurements”, PhD thesis, University of Konstanz. Cuvillier: Göttingen, 2003

[11] H. Plagwitz, and R. Brendel, “Analytical Model for the diode saturation current of point-contacted solar cells”, Progress in Photovoltaics: Research and Applications, 2006, **14**: 1-12

[12] R. Brooks, and H. Mattes, “Spreading resistance between constant potential surfaces”, Bell Systems Technical Journal 1971; **50**: 775–785